

Infrared transmission spectroscopy of charge carriers in self-assembled InAs quantum dots under surface electric fields

Shovon Pal^{1,2}, Sascha R Valentin¹, Nadezhda Kukharchyk¹,
Hanond Nong², Alireza B Parsa³, Gunther Eggeler³, Arne Ludwig¹,
Nathan Jukam² and Andreas D Wieck¹

¹ Lehrstuhl für Angewandte Festkörperphysik, Ruhr-Universität Bochum, D-44780 Bochum, Germany

² AG Terahertz Spektroskopie und Technologie, Ruhr-Universität Bochum, D-44780 Bochum, Germany

³ Institut für Werkstoffe, Ruhr-Universität Bochum, D-44780 Bochum, Germany

E-mail: shovon.pal@ruhr-uni-bochum.de

Received 26 September 2014, revised 29 October 2014

Accepted for publication 30 October 2014

Published 24 November 2014

Abstract

We present a study on the intersublevel spacings of electrons and holes in a single layer of InAs self-assembled quantum dots. We use Fourier transform infrared transmission spectroscopy via a density chopping scheme for direct experimental observation of the intersublevel spacings of electrons without any external magnetic field. Epitaxial, complementary-doped and semi-transparent electrostatic gates are grown within the ultra high vacuum conditions of molecular beam epitaxy to voltage-tune the device, while a two dimensional electron gas (2DEG) serves as a back contact. Spacings of the hole sublevels are indirectly calculated from the photoluminescence spectrum by using a simple model given by Warburton *et al* [1]. Additionally, we observe that the intersubband resonances of the 2DEG are enhanced due to the quantum dot layer on top of the device.

Keywords: intersublevel spacings, quantum dots, 2DEG, epitaxial gates, FTIR transmission spectroscopy

(Some figures may appear in colour only in the online journal)

Quantum-confined zero-dimensional semiconductor quantum dots (QDs) have attracted unparalleled interest for more than a decade [2, 3]. These nanostructures have an immense potential for device applications ranging from simple electronic memories [4] to novel optoelectronics [5]. The novelty can be extended by combining a quantum well (QW) with these zero-dimensional systems. Tunneling dynamics (refilling times) of electrons from QW to QD are tunable from μs to ms by changing the barrier thickness between them [2, 6].

Electronic read-out of memory devices based on self-assembled quantum dots (SAQDs) demands an effective electrical control over the device. One of the first experiments towards this goal was performed by Sakaki *et al* [7], where they studied the transport properties of two dimensional electron gas (2DEG) with embedded InAs QDs. Much work has been done to study the changes in conductance, carrier concentration and mobility of the 2DEG due to successive charging of QD levels [8, 9]. Electrostatic

quantization results in the formation of quasi-two-dimensional electron or hole states called subbands or sublevels. The spacing between the subbands is an important parameter defining device applications. Intersublevel spacings in InAs SAQD infrared photodetectors were determined using infrared photoconductivity measurements [10, 11]. Besides, much investigation has been carried out on the intersubband transitions of the 2DEG using grating couplers [12]. However, questions arising on the influence of QDs on the intersubband spacings of the 2DEG and vice-versa in coupled nanostructures have not been addressed. Several theoretical models [13, 14] are proposed to study the sublevel spacings. Nevertheless, due to lack of experimental agreement, determination of such energetic spacings still remains a subject of intense research.

In this paper, we address these questions and study in depth the intersublevel spacings in QDs and their influence on the 2DEG intersubband spacing by Fourier transform infrared (FTIR) transmission spectroscopy via a density

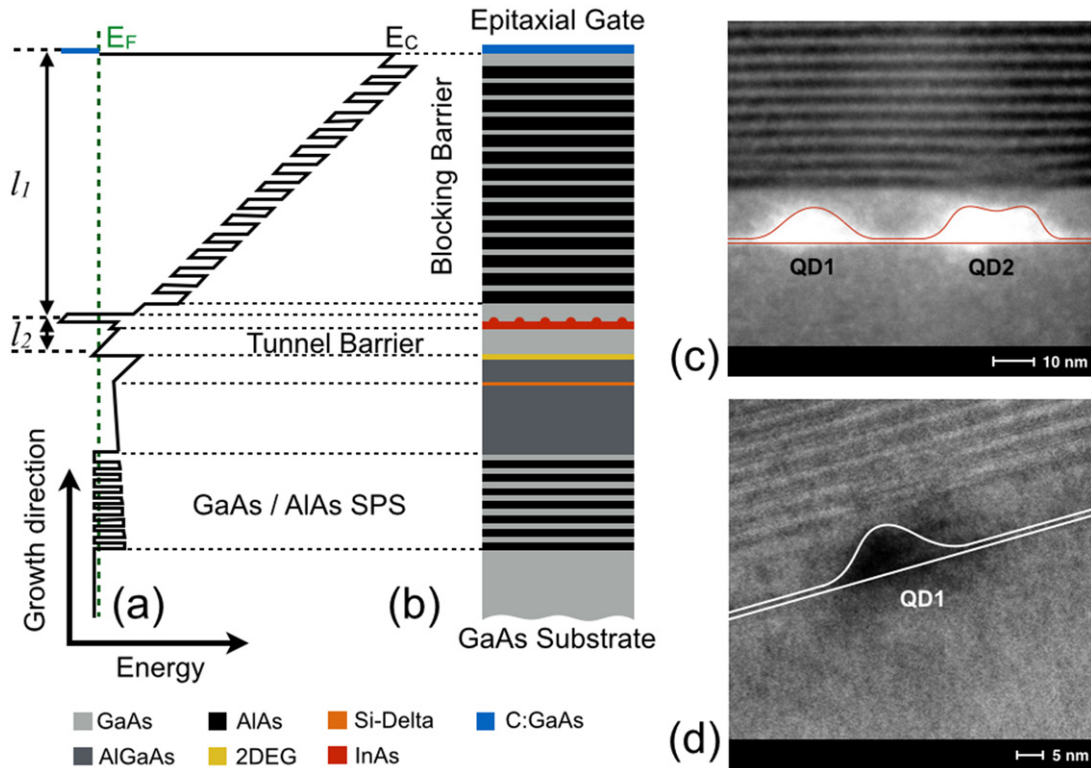


Figure 1. (a) Sketch of the conduction band edge E_c , when no QD level is filled with electrons. l_1 is the distance of the QD from the gate (246 nm) and l_2 is the thickness of the tunnel barrier (30 nm). (b) Schematic of the layer sequence of the sample. (c) STEM image of the two QDs spaced apart by 44 nm. QD1 has a base diameter of 27 nm and height of 8 nm and QD2 has a base diameter of 30 nm and height of approximately 8 nm. An imprint of strain relaxation is observed through the first three periods of SPS over QD2. (d) TEM image of QD1, where the dark feature represents the QD. The additional white lines are markers.

chopping scheme without applying any external magnetic field. This spectroscopy is done together with capacitance-voltage (C-V) spectroscopy in order to determine the voltages used in the density chopping scheme and photoluminescence (PL) spectroscopy to study the interband transitions in the QDs. We also study the sublevel spacing of holes in the valence band of InAs SAQDs. We show the successful implementation of epitaxial, complementary-doped and semi-transparent electrostatic gates, for the first time, to replace the conventional Schottky gates.

The investigated sample is grown on a semi-insulating GaAs (100) substrate using molecular beam epitaxy (MBE). Figure 1(b) schematically shows the layer sequence of the sample. An inverted high electron mobility transistor (iHEMT) structure is fabricated, on top of which InAs SAQDs are realized by Stranski-Krastanov growth mode with a nominal thickness of 2.2 monolayers (MLs), separated from the 2DEG by a tunnel barrier of a 30 nm thick GaAs layer. The QDs are then capped by 11 nm GaAs followed by a blocking barrier, which consists of 50 periods of AlAs/GaAs (3 nm/1 nm) short-period-superlattice (SPS). An epitaxial, complementary-doped and semi-transparent electrostatic gate is grown on top of the sample within the ultra high vacuum conditions of the MBE. It is composed of a 25 nm thick bulk carbon-doped GaAs layer ($N_A = 3 \times 10^{18} \text{ cm}^{-3}$), followed by 40 periods of carbon-delta-doped and 0.5 nm carbon-doped GaAs layers ($N_A = 1 \times 10^{19} \text{ cm}^{-3}$).

The carrier concentration of the epitaxial gate, obtained from Hall measurements, shows values of approximately $6 \times 10^{18} \text{ cm}^{-3}$. There are a couple of advantages for using such gates. First, these gates have better optical transmission and do not suffer from low breakdown voltages in comparison to Schottky gates. Second, they grow lattice-matched and hence induce minimal strain on the underlying semiconductor layer. A sketch of the conduction band edge is shown in figure 1(a). The scanning transmission electron microscope (STEM) image in figure 1(c) shows a cross-sectional view of typical QDs in the QD-ensemble of our device. Two QDs labeled as QD1 and QD2 show a variation in their shape. A visible change in the morphology is observed in the first three SPS over QD2 due to strain relaxation. The two dots are separated by 44 nm, however the dot period in the structure is random. An inverted etch-mask with an array of different dimensions ranging from $200 \times 200 \mu\text{m}^2$ to $500 \times 500 \mu\text{m}^2$ is used to prepare gates on top of the sample. The four corners of the sample are further etched by 200 nm and Indium is diffused in an inert atmosphere of Hydrogen and Nitrogen (also known as forming gas) to contact the 2DEG layer and prevent oxidation.

Interband spacings between the sublevels of electrons and holes in the InAs SAQDs (shown in figure 2) are characterized by photoluminescence measurements at three different temperatures. A modulated laser diode, which emits at 638 nm (1.94 eV), is used to excite the sample and a liquid-nitrogen-cooled InGaAs photodiode is used as a detector.

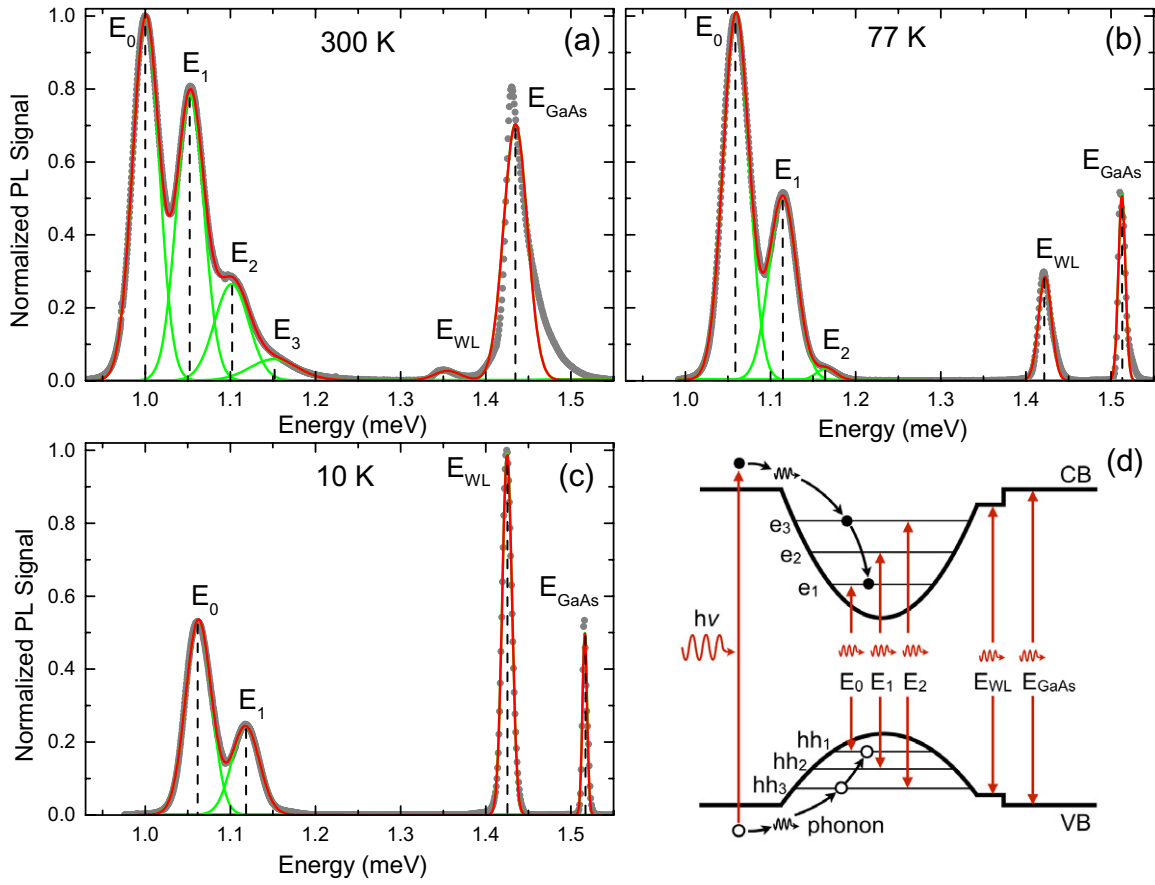


Figure 2. (a) Room temperature, 300 K, (b) 77 K and (c) 10 K photoluminescence spectra measured with an excitation power of 5 mW. Spectral deconvolutions are plotted in green. The experimental data points are plotted in grey dots and the reconstructed spectra are shown in red. (d) Schematic representation of the transitions corresponding to each peak.

The photo-generated electrons and holes undergo energy and momentum relaxation towards the band-gap minima, where they finally recombine and emit photons with energies given by [14]

$$E_i = E_g - E_{e_{i+1}} - E_{hh_{i+1}} - E_{x_i}, \quad (1)$$

where i represents the index of the levels, E_g is the band-gap of the matrix material (GaAs), $E_{e_{i+1}}$ and $E_{hh_{i+1}}$ are the energetic distances in the conduction and valence band measured from the respective edges of the GaAs band and E_{x_i} is the exciton binding energy. Figure 2(d) shows the schematic of the interband transitions in the QD. At 300 K, four interband transitions in QDs are observed (figure 2(a)), marked as E_0 , E_1 , E_2 and E_3 along with the transitions in the wetting layer (E_{WL}) and GaAs (E_{GaAs}). With decreasing the temperature to 77 K, the respective transitions shift to higher energies (figure 2(b)) according to Varshni’s empirical relation [15]. Further decreasing the temperature to 10 K, only two distinct interband transitions are visible (figure 2(c)), marked as E_0 (1.062 eV) and E_1 (1.118 eV), together with the transitions in the wetting layer and GaAs. Values of QD interband transitions at three different temperatures along with their full width at half maximum (FWHM) are given in table 1.

We observe an increase in the non-normalized peak intensity of E_0 (not shown) by 50% from 300 K to 10 K. While

Table 1. Deconvolution results of the PL spectra at different temperatures. The values in the brackets are the FWHM of the respective peaks. All values are in eV.

Peaks	300 K	77 K	10 K
E_0	1.001 (0.036)	1.059 (0.036)	1.062 (0.036)
E_1	1.053 (0.038)	1.114 (0.038)	1.118 (0.038)
E_2	1.102 (0.047)	1.165 (0.027)	—
E_3	1.151 (0.066)	—	—
E_{WL}	1.355 (0.035)	1.422 (0.018)	1.425 (0.013)
E_{GaAs}	1.435 (0.033)	1.512 (0.009)	1.516 (0.006)

the intensity of E_1 does not change during cooling, E_2 and E_3 disappear. On the other hand, a strong emission from the wetting layer is observed at 10 K as compared to the emission at 300 K (clearly seen from the normalized spectra in figure 2). The disappearance of E_2 and E_3 and the increase of emission from the wetting layer can be explained as follows: At low temperatures, the charge carriers in the QDs thermalize to the ground state. Also, the carriers in the wetting layer are thermalized quickly. This reduces the capture of the carriers from the wetting layer because the barrier around the QDs cannot be overcome due to low kinetic energies of the carriers. As a consequence, the number of excited state transitions is also reduced, as seen at 10 K. Moreover, the broadening of the peaks can also be assisted to the fact that Stranski–Krastanov

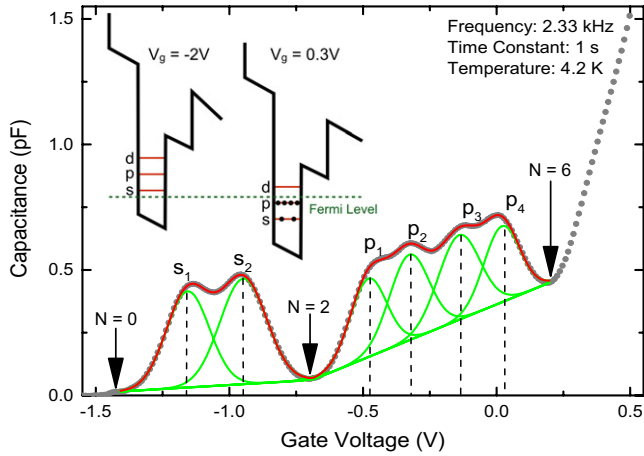


Figure 3. Capacitance measured as a function of the gate voltage at 4.2 K. The capacitance is corrected by subtracting the linear slope. Successive charging of QD levels is observed on increasing the gate voltage. The green gaussian curves indicate the deconvoluted peaks corresponding to the filling of electrons in the QD levels. The red curve represents the reconstructed spectrum from $V_g = -1.4$ V to $V_g = 0.25$ V. Inset: Band-schematic illustrating the QD levels with respect to the Fermi level for two gate voltages.

growth of QDs leads to an ensemble resulting in a sum of the emission of QDs of different sizes [16].

On varying the gate voltage (V_g) from -2 V to 1 V, we inject electrons from the back-contact (2DEG) into the InAs QDs through the GaAs tunnel barrier. The charging of the QD level with an electron is observed as a change in the capacitance between the top gate and the back contact. Figure 3 shows the variation of capacitance with the gate voltage at 4.2 K. A small sine signal of 10 mV and 2.33 KHz is used as a modulation for the DC voltage. In the inset of figure 3, schematics of the QD levels are shown for two different voltages. At -2 V, no QD levels are occupied and hence this voltage is chosen as a reference voltage (V_r). With sufficient forward bias (0.3 V), we see the occupation of s -sublevel, which is two-fold degenerate, and p -sublevel, which is four-fold degenerate. At an intermediate voltage of -0.55 V, only the s -sublevel is occupied. The density of QDs can be obtained by using the relation [17]:

$$N_{\text{QD}} = \frac{1}{2eA} \cdot \frac{l_1 + l_2}{l_2} \int_{-1.5}^{-0.7} C(V) dV, \quad (2)$$

where N_{QD} is the density of QDs, $(l_1 + l_2)/l_2$ is given by the lever-arm rule (for values of l_1 and l_2 , see caption of figure 1(a)) and A ($500 \times 500 \mu\text{m}^2$) is the area of the gate. The integration is performed between the voltage limits where only the s -sublevel is occupied. The density of the QDs calculated from the CV spectrum using equation (2) is $2 \times 10^9 \text{ cm}^{-2}$. The corresponding gate voltages can be converted to the respective electrostatic energies by employing the lever-arm rule as described in [17]. These values are given in table 2. The energetic spacing between the s - and p -sublevels of the QD can be evaluated as follows: The difference between the s_2 and p_1 peaks is equal to the sum of the sublevel resonance

Table 2. Energies corresponding to the individual electron charging peaks in the C-V spectrum. The voltages are taken from the deconvolution result of the complete spectrum. The values in the brackets represent the energy difference between the given peak and the consecutive peak before.

Charging peaks	Gate voltage (V)	Energy (lever arm) (meV)
s_1	-1.156	223.1
s_2	-0.948	200.5 (22.6)
p_1	-0.480	149.8 (50.7)
p_2	-0.327	133.2 (16.6)
p_3	-0.141	112.9 (20.3)
p_4	0.019	95.5 (17.4)

energy and one-fourth of the Coulomb energy, given as [11]

$$E_{s_2} - E_{p_1} = E_{s \rightarrow p} + \frac{1}{4} E_{\text{Coulomb}}, \quad (3)$$

where $E_{s_2} - E_{p_1} = 50.7$ meV, $E_{s \rightarrow p}$ is the spacing between the s - and p -sublevels and $E_{\text{Coulomb}} = 22.6$ meV is the Coulomb blockade energy ($E_{s_1} - E_{s_2}$, see table 2). Using these values, we obtain an energetic spacing of 45.1 meV between the s - and p -sublevel. However, this method is not a direct observation of the intersublevel spacings in the QDs.

Direct investigation of the quantized energy levels within the conduction band is performed by infrared transmission measurements with a rapid scan Bruker IFS113V interferometer, which has two sources (mercury-arc lamp and global) to cover a large range of infrared radiation. The spectral resolution of the measurements is 0.25 cm^{-1} ($=0.03$ meV). The bottom surface of the sample is wedged at around 3° to avoid the Fabry-Perot interference fringes and mounted at an angle of 30° (obeying the polarization selection rule for observing the intersubband transitions) in a self-built cryogenic optical sample holder, which is equipped with a liquid-Helium cooled Si-bolometer for detection. Spectra at a certain gate voltage and reference voltage are collected alternatively and averaged over long measurement times (3 h) to rule out the long-term experimental drifts [18]. The normalized transmission, $T(V_g)/T(V_r)$, is given by [19]:

$$\frac{T(V_g)}{T(V_r)} = 1 - \frac{2\text{Re}[\sigma(\omega)]}{(1 + \sqrt{\varepsilon} + r_v/r_g)\varepsilon_0 c}, \quad (4)$$

where ε_0 is the permittivity of free space, c is the velocity of light, ε is the dielectric constant of InAs, $r_v = 377 \Omega$ is the vacuum impedance and $r_g = 12 \text{ K}\Omega$ is the combined impedance of the epitaxial gate and the back-contact at 4.2 K. The high-frequency conductivity, $\sigma(\omega)$, of electrons in a parabolic potential is

$$\sigma(\omega) = \frac{Ne^2\tau}{2m^*a^2 \left[1 + i \frac{(\omega^2 - \omega_r^2)\tau}{\omega} \right]}, \quad (5)$$

where ω_r is the high-frequency resonance, a is the average QD periodicity and τ is the scattering time, which basically determines the line-width of the transitions. Theoretical curves generated by using equation (4) show close correspondence

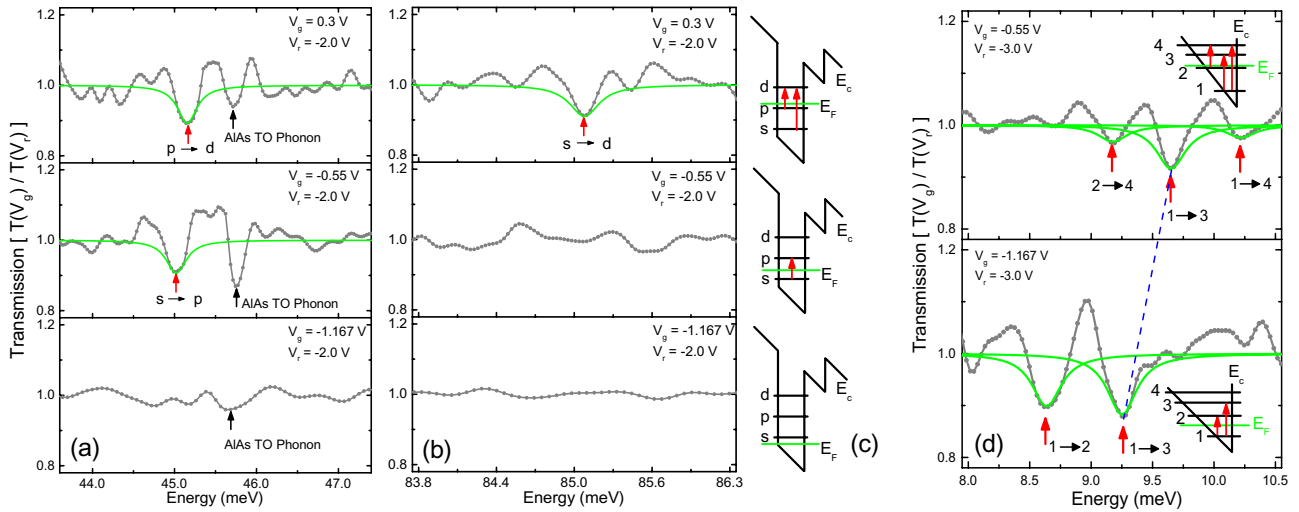


Figure 4. Transmission spectra at three different gate voltages each normalized to the threshold voltage (no carriers induced) of -2 V. (a) At -1.167 V, only an absorption due to AlAs TO-phonon (45.7 meV) is observed. At -0.55 V, $s \rightarrow p$ transition is recorded at 45.0 meV along with the enhanced TO-phonon absorption at 45.7 meV. At 0.3 V, $p \rightarrow d$ transition is observed at 45.1 meV along with the TO-phonon absorption at 45.7 meV. (b) Transmission spectra at higher frequencies than in (a): At 0.3 V, $s \rightarrow d$ transition is recorded at 85.1 meV. (c) The level schemes for the respective transitions observed in (a) and (b). (d) Optically enhanced intersubband transitions in the 2DEG for two gate voltages at substantially lower frequencies than that of QDs in (a) and (b). The resonances shift to higher energies as the carrier density increases with the gate voltage. One such shift is shown by the blue dashed line. The grey curves represent the experimental spectra and the green curves represent the simulated transmission spectra.

to the experimental data. These are shown as green curves in figure 4. At $V_g = -1.167$ V, we observe only a small dip in the transmission due to the AlAs TO-phonon at 45.7 meV [20]. At $V_g = -0.55$ V, electrons from the s -sublevel absorb the incident infrared radiation and occupy the next sublevel with a minimum in the transmission spectra at 45.0 meV ($s \rightarrow p$), as compared to 45.1 meV calculated from the C-V measurements. Upon increasing the voltage to 0.3 V, when both s - and p -sublevels are occupied, transitions from both the levels to the d -sublevel are registered as minima in the transmission spectrum at 45.1 meV ($p \rightarrow d$) and 85.1 meV ($s \rightarrow d$), respectively. For $s \rightarrow d$, the value is almost twice the value observed in $s \rightarrow p$ or $p \rightarrow d$. This is expected to a very good approximation for confinement due to parabolic potential leading to equidistant levels. However, the small variation is due to the fact that at 0.3 V the p -sublevel is also filled, leading to additional interactions, which reduce the energy. We also observe a large coupling of $s \rightarrow p$ and $p \rightarrow d$ transitions to the AlAs TO-phonon (45.7 meV). The coupling effect can be seen in figure 4(a) as an increase in the transmission depth of the phonon transition at 45.7 meV when a bias of -0.55 V or 0.3 V is applied as compared to the case when no transitions in QDs are observed at -1.167 V. This is an interesting feature resulting from the close vicinity of AlAs in the SPS to the QDs, separated by less than 5 nm. Using the results from PL spectra and the simple model given by Warburton *et al* [1], we calculate the sublevel spacing of the holes in the valence band. The energetic distance between hh_1 and hh_2 (see figure 2(d)) is found to be 10.9 meV. However, it is to be noted that our device structure is more complicated as compared to the one considered for developing the simple model in [1], resulting in additional complex electrostatics. The calculated hole spacing shows very close correspondence to the observed

experimental value performed by Jang *et al* [21] via excitation-power dependence of PL spectrum for an n -modulation-doped QD structure. On the contrary, this value is small compared to the values in [22, 23], where they state that the hole sublevel spacing is in the order of 20–25 meV. Clearly, this is a riddle, which can be solved by direct access to hole sublevels via FTIR measurements on p -type samples.

At lower frequencies, strong intersubband resonances (ISRs) are observed in the 2DEG. The 2D electron density obtained from Hall measurements is $3 \times 10^{11} \text{ cm}^{-2}$. Sufficient negative bias ($V_t = -3$ V) is applied to completely deplete the 2DEG below the threshold voltage, which is used as reference for the chopping scheme. The strong enhancement of the 2DEG-ISRs is due to the layer of QDs on top, which helps in better coupling of the incident radiation with the intersubband transitions of the 2DEG. This is due to the fact that the InAs SAQDs in the GaAs matrix act analogous to a grating coupler, which tilts locally the electric field vector of the incident wave, leading to substantial components in the growth direction (normal to the 2DEG), which is necessary to excite ISR. As a consequence, we observed around 6% transmission dip in the primary ISR as compared to the strengths of the transitions reported previously 1–2% [12]. With an increase in the gate voltage, the ISR shifts to higher energies owing to an increase in the carrier density steepening up the asymmetric triangular potential, which confines the 2DEG and thus leading to higher intersubband spacings.

The picture is however not that simple, since many-electron interactions significantly change the single electron intersubband transition energies of the 2DEG in a HEMT structure. Under the local density approximation and linear response theory, it was shown by Ando [24] that the two most significant contributions are the depolarization effect which blue-shifts the ISR and the exciton-like effect which red-shifts

the ISR. Besides, with an increase in the voltage (-0.55 V), the QDs are also charged and this will result in an additional field across the 2DEG layer. The resonances observed are a result of the combined effect of the above mentioned phenomena.

An interesting feature observed in the electronic sublevel resonances in the SAQDs via FTIR measurements is their linewidths which are as narrow as $2-3$ meV in comparison to the linewidths seen in the C-V spectrum. We observed considerable fluctuations of the thickness of the QDs in the growth direction from the STEM and TEM images (not shown). This significantly affects the ground state energy, which broadens the charging spectrum in the C-V measurements. However, the influence on the energetic spacings of *s*-, *p*- and *d*-sublevels is very small, leading to narrow linewidths in the FTIR spectra. The stability in the confining potential allows us to observe the discrete sublevel resonances in the transmission spectra of FTIR measurements, even though our experiments are performed over an ensemble of QDs [11]. Apparently, this unique property of the SAQDs has been perfected and employed over the years for device applications like QD-lasers, QD-infrared photodetectors etc.

In conclusion, the use of epitaxial, complementary doped and semi-transparent electrostatic gates to chop the density of charge carriers proved to be an efficient technique to study the intersublevel spacings of electrons in the conduction band. Using these results along with the interband transition values from PL, we evaluated the sublevel spacing of the holes in the valence band. We found that the simulated transmission spectra correspond to a very good approximation to the experimental observations. We also found a good agreement between the values of intersublevel spacings calculated indirectly from the C-V measurement with the value from the infrared transmission measurements via chopping scheme. Due to the coupled structure with the QD layer on top, the 2DEG intersubband resonances were strongly enhanced. Moreover, there was no visible coupling of the intersubband resonances of the 2DEG and the intersublevel transitions in the QDs and they are well separated by the Reststrahlen band of GaAs. However, due to the close vicinity of the SPS to the QDs, a large coupling was observed between the AlAs TO phonon and the intersublevel transitions in the QDs. Interesting features of SAQDs were seen in the STEM images, for example the change in the morphology of the SPS due to strain relaxation.

Acknowledgments

We would like to thank D Heitmann, R Blick, U Merkt and W Hansen from the university of Hamburg for

providing the BrukerIFS113V spectrometer used in this work. The work was financially supported by IMPRS-SurMat, MPIE Düsseldorf, BMBF Quantum communication program—Q.com-H 16KIS0109 and BMBF-QUIMP 16BQ1062 as well as Mercur Pr-2013-0001. The authors would also like to acknowledge the DFH/UFA CDFA-05-06 Nice-Bochum and the RUB Research School.

References

- [1] Warburton R J, Miller B T, Dürr C S, Bödefeld C, Karrai K, Kotthaus J P, Madeiros-Ribeiro G, Petroff P M and Huan T S 1998 *Phys. Rev. B* **58** 16221
- [2] Cerulo G, Nevou L, Liverini V, Castellano F and Faist J 2012 *J. Appl. Phys.* **112** 043702
- [3] Lorke A, Kotthaus J P and Ploog K 1990 *Phys. Rev. Lett.* **64** 2559
- [4] Kannan E S, Kim G-H and Ritchie D A 2009 *Appl. Phys. Lett.* **95** 143506
- [5] Bhattacharya P and Mi Z 2007 *Proc. IEEE*. **95** 1723
- [6] Nevou L, Liverini V, Castellano F, Bismuto A and Faist J 2010 *Appl. Phys. Lett.* **97** 023505
- [7] Sakaki H, Yusa G, Someya T, Ohno Y, Noda T, Akiyama H, Kadoya Y and Noge H 1995 *Appl. Phys. Lett.* **67** 3444
- [8] Marquardt B, Geller M, Lorke A, Reuter D and Wieck A D 2009 *Appl. Phys. Lett.* **95** 022113
- [9] Marquardt B, Beckel A, Lorke A, Wieck A D, Reuter D and Geller M 2011 *Appl. Phys. Lett.* **99** 223510
- [10] Meurer B, Heitmann D and Ploog K 1992 *Phys. Rev. Lett.* **68** 1371
- [11] Drexler H, Leonard D, Hansen W, Kotthaus J P and Petroff P M 1994 *Phys. Rev. Lett.* **73** 2252
- [12] Wieck A D, Thiele F, Merkt U, Ploog K, Wiemann G and Schlapp W 1989 *Phys. Rev. B* **39** 3785
- [13] Grundmann M, Stier O and Bimberg D 1995 *Phys. Rev. B* **52** 11969
- [14] Bimberg D, Grundmann M and Ledentsov N N 1999 *Quantum Dot Heterostructures* (New York: Wiley)
- [15] Varshni Y P 1967 *Physica* **34** 149
- [16] Petroff P M and DenBaars S P 1994 *Superlatt. Microstruct.* **15** 15
- [17] Wang Z M 2008 *Self-Assembled Quantum Dots* (New York: Springer) pp 337–57
- [18] Batke E and Heitmann D 1984 *Infrared Phys.* **24** 189
- [19] Wilson B A, Allen S J Jr and Tsui D C 1981 *Phys. Rev. B* **24** 5887
- [20] Giannozzi P, Gironcoli S, Pavone P and Baroni S 1991 *Phys. Rev. B* **43** 7231
- [21] Jang Y D, Yim J S, Lee D, Kim G-H, Liang C-T, Farrer I and Ritchie D A 2005 *Appl. Phys. Lett.* **87** 232110
- [22] Reuter D, Kailuweit P, Wieck A D, Zeitler U, Wibbelhoff O, Meier C, Lorke A and Mann J C 2005 *Phys. Rev. Lett.* **94** 26808
- [23] Stauber T and Zimmermann R 2006 *Phys. Rev. B* **73** 115303
- [24] Ando T 1977 *Solid State Commun.* **21** 133